

Differentiating CDM and Baryon Isocurvature Models with 21 cm Fluctuations

Masahiro Kawasaki^{1,2}, Toyokazu Sekiguchi^{1,3} and Tomo Takahashi⁴

¹*Institute for Cosmic Ray Research, University of Tokyo, Kashiwa 277-8582, Japan*

²*Institute for the Physics and Mathematics of the Universe, University of Tokyo, Kashiwa, Chiba, 277-8568, Japan*

³*Department of Physics and Astrophysics, Nagoya University, Nagoya 464-8602, Japan*

⁴*Department of Physics, Saga University, Saga 840-8502, Japan*

Abstract

We discuss how one can discriminate models with cold dark matter (CDM) and baryon isocurvature fluctuations. Although current observations such as cosmic microwave background (CMB) can severely constrain the fraction of such isocurvature modes in the total density fluctuations, CMB cannot differentiate CDM and baryon ones by the shapes of their power spectra. However, the evolution of CDM and baryon density fluctuations are different for each model, thus it would be possible to discriminate those isocurvature modes by extracting information on the fluctuations of CDM/baryon itself. We discuss that observations of 21 cm fluctuations can in principle differentiate these modes and demonstrate to what extent we can distinguish them with future 21 cm surveys. We show that, when the isocurvature mode has a large blue-tilted initial spectrum, 21 cm surveys can clearly probe the difference.

1 Introduction

Current cosmological observations are now very precise to give a stringent constraint on the adiabaticity of density fluctuations. However, some contribution of non-adiabatic fluctuations, so-called isocurvature fluctuations, is still allowed (see e.g., [1]). Isocurvature fluctuations can be generated in cold dark matter (CDM) and baryon sectors, from which we can have some insight on the nature of dark matter and/or the mechanism of the baryogenesis. This is because isocurvature fluctuations might be produced depending on how dark matter/baryon number is generated. Such examples are axion [2–8] and Affleck-Dine baryogenesis mechanism [9–12] in which CDM and baryon isocurvature fluctuations can respectively be generated^{#1}. If such a mode is found to be non-zero, it would give invaluable information on CDM/baryogenesis scenarios.

Currently, stringent constraints on isocurvature fluctuations come from cosmic microwave background (CMB) observations such as WMAP [1]. However, CMB cannot discriminate CDM and baryon ones since these two isocurvature modes give indistinguishable CMB angular power spectra. The initial non-zero isocurvature mode of CDM/baryon affects fluctuations of photons, at which we are looking in CMB observations, only through gravity. CDM and baryon can be regarded as the same component as far as the gravity is concerned, hence the effects of isocurvature fluctuations arise in exactly the same way for CMB anisotropy (except the amplitude which depends on the amount of CDM and baryon).

Thus even if we see some signature of existence of the isocurvature mode from CMB measurements, we cannot tell whether CDM or baryon is responsible for that. From the viewpoint of testing dark matter models/baryogenesis mechanism, it is very crucial to differentiate these two modes in some way, which is the issue we are going to discuss in this paper. Although CMB measurement cannot do this task, the evolution of density fluctuations of CDM and baryon themselves are not the same for models with initial CDM and baryon isocurvature fluctuations. Thus we may have some possibility for differentiating those by looking at (CDM/baryon) fluctuations directly.

In this paper, we discuss how one can probe the difference between these two isocurvature modes by using observations of fluctuations in redshifted 21 cm line absorption. As mentioned above, CDM and baryon fluctuations evolve differently when one assume different isocurvature modes (i.e., CDM and baryon ones). Hence, if either one can be probed directly in some way, we can in principle see the difference. Since 21 cm fluctuations effectively probe baryon density fluctuations, the observations of them can be utilized for this purpose^{#2}.

^{#1} Other examples producing CDM/baryon isocurvature fluctuations include the curvaton model [13–15], in which the isocurvature fluctuations partially/totally correlated with adiabatic ones depending on how CDM/baryon are generated [16, 17]. Furthermore, isocurvature fluctuations can be generated in neutrino density fluctuations and neutrino velocity [18]. However, we focus on uncorrelated CDM and baryon isocurvature modes in this paper.

^{#2} The possibility of probing baryon and CDM fluctuations separately using 21 cm fluctuations was discussed in [19]. The issue of distinguishing baryon and CDM isocurvature modes with 21 cm surveys

The organization of this paper is as follows. In the next section, we discuss the evolution and effects of density fluctuations of CDM and baryon in models with isocurvature fluctuations. We explain in some detail what aspect differs between CDM and baryon isocurvature modes by looking at density fluctuations of CDM and baryon in these modes. Then in Section 3, we show that 21 cm fluctuations can in principle differentiate the CDM and baryon isocurvature modes, which is impossible with CMB observations. We also demonstrate a future constraint on CDM and baryon isocurvature fluctuations by utilizing future 21 cm survey and discuss to what extent they can be discriminated. The final section is devoted to the summary of this paper.

2 Evolutions of density fluctuations in CDM and baryon isocurvature models

2.1 Notations

Before we start the discussion on the evolution of density fluctuations, here we give some definitions, in particular, regarding isocurvature fluctuations to set our notation.

Gauge-invariant isocurvature fluctuations between the components i and j are defined as

$$S_{ij} = -3H \left(\frac{\delta\rho_i}{\dot{\rho}_i} - \frac{\delta\rho_j}{\dot{\rho}_j} \right). \quad (1)$$

In the following, we mainly consider isocurvature fluctuations of CDM and baryon with respect to radiation, which we write as

$$S_c = \delta_c - \frac{3}{4}\delta_\gamma, \quad S_b = \delta_b - \frac{3}{4}\delta_\gamma. \quad (2)$$

Furthermore, in this paper we only consider uncorrelated type of isocurvature fluctuations. Thus CDM and baryon isocurvature modes can be respectively identified as the ones with non-vanishing $S_c = \delta_c(\tau \rightarrow 0)$ and $S_b = \delta_b(\tau \rightarrow 0)$, with τ being the conformal time, at the early times when the initial conditions are set for cosmological density fluctuations. Then the primordial power spectrum for isocurvature fluctuations is defined as

$$\mathcal{P}_{S_i}(k)(2\pi)^3\delta^{(3)}(\mathbf{k} - \mathbf{k}') = \frac{k^3}{2\pi^2} \langle S_i(\mathbf{k})S_i(\mathbf{k}')^* \rangle, \quad (3)$$

where $i = c$ and b indicating CDM and baryon, respectively, and we parametrize \mathcal{P}_{S_i} as

$$\mathcal{P}_{S_i}(k) = \mathcal{P}_{S_i}(k_0) \left(\frac{k}{k_0} \right)^{n_s^{(i)} - 1} \quad (4)$$

was investigated for the ‘‘compensated isocurvature mode’’ in [20]. See also [21].

with $n_s^{(i)}$ is the spectral index for the mode i . In this paper, we take the reference scale k_0 as $k_0 = 0.002 \text{ Mpc}^{-1}$. For CDM and baryon isocurvature modes, we denote it as $n_s^{(\text{CDMiso})}$ and $n_s^{(\text{biso})}$, respectively. For the adiabatic (curvature) fluctuations, similarly to the above, one usually defines as

$$\mathcal{P}_\zeta(k)(2\pi)^3\delta^{(3)}(\mathbf{k} - \mathbf{k}') = \frac{k^3}{2\pi^2} \langle \zeta(\mathbf{k})\zeta(\mathbf{k}')^* \rangle, \quad (5)$$

where ζ is the curvature perturbation and the power spectrum \mathcal{P}_ζ can also be written as

$$\mathcal{P}_\zeta(k) = \mathcal{P}_\zeta(k_0) \left(\frac{k}{k_0} \right)^{n_s-1}, \quad (6)$$

with n_s being the spectral index for the adiabatic mode.

Current cosmological observations such as WMAP indicate that cosmic density fluctuations are almost adiabatic and pure isocurvature fluctuations of any modes are excluded. However, some fraction (contamination) of isocurvature fluctuations are still allowed. To characterize the fractions of the isocurvature modes, we define the quantities r_a and r_b as^{#3}

$$r_c \equiv \frac{\mathcal{P}_{S_c}(k_0)}{\mathcal{P}_\zeta(k_0)}, \quad r_b \equiv \frac{\mathcal{P}_{S_b}(k_0)}{\mathcal{P}_\zeta(k_0)}. \quad (8)$$

From current observations, r_c is constrained to be less than about 10 % [1]. (The corresponding constraint on r_b becomes less severe by the factor of $(\Omega_c/\Omega_b)^2$.) Thus we use $r_c = 0.1$ as a reference value unless otherwise stated in the following.

2.2 Evolutions of density fluctuations

Now we study the evolutions of density fluctuations in models with CDM and baryon isocurvature fluctuations and see the difference of those between in these isocurvature modes, which could be probed with 21 cm fluctuations. In addition, we also discuss why CMB cannot discriminate these two isocurvature modes at linear perturbation level.

In the following, we investigate density perturbations in the synchronous gauge where the metric perturbations are defined as

$$ds^2 = a^2(\tau)[-d\tau^2 + (\delta_{ij} + h_{ij})dx^i dx^j], \quad (9)$$

with

$$h_{ij}(\mathbf{x}, \tau) = \int dk^3 e^{i\mathbf{k}\cdot\mathbf{x}} \left[\hat{\mathbf{k}}_i \hat{\mathbf{k}}_j h(\mathbf{k}, \tau) + \left(\hat{\mathbf{k}}_i \hat{\mathbf{k}}_j - \frac{1}{3}\delta_{ij} \right) 6\eta(\mathbf{k}, \tau) \right]. \quad (10)$$

^{#3} In some literature such as [1, 22], the fraction of isocurvature fluctuations is defined as

$$\alpha = \frac{\mathcal{P}_{S_c}(k_0)}{\mathcal{P}_\zeta(k_0) + \mathcal{P}_{S_c}(k_0)}, \quad (7)$$

which is a bit different from the one used here. However, as far as the fraction of the isocurvature fluctuations is small, both definitions are almost equivalent.

Here τ is the conformal time and a is the scale factor. We denote density fluctuations of a species i as $\delta_i \equiv \delta\rho_i/\bar{\rho}_i$. In particular, here we study those of CDM δ_c , baryon δ_b and photons δ_γ . We follow the notation of [23].

In this gauge, the perturbed Einstein equations are:

$$k^2\eta - \frac{1}{2}\mathcal{H}\dot{h} = -4\pi Ga^2\delta\rho, \quad (11)$$

$$k^2\dot{\eta} = -4\pi Ga^2(\bar{\rho} + \bar{P})\theta, \quad (12)$$

$$\ddot{h} + 2\mathcal{H}\dot{h} - 2k^2\eta = -24\pi Ga^2\delta P, \quad (13)$$

$$\ddot{h} + 6\ddot{\eta} + 2\mathcal{H}(\dot{h} + 6\dot{\eta}) - 2k^2\eta = -24\pi Ga^2(\bar{\rho} + \bar{P})\sigma, \quad (14)$$

where a dot represents the derivative with respect to the conformal time τ and $\mathcal{H} = \dot{a}/a$ is the Hubble parameter defined with the conformal time derivative. $\delta\rho$ and δP are fluctuations of energy density and pressure for the total component. θ is a variable defined as $(\bar{\rho} + \bar{P})\theta = \sum_i(\bar{\rho}_i + \bar{P}_i)ikv_i$ with v_i being velocity perturbation of species i and σ represents the anisotropic stress of the total component. The equation for the CDM fluctuations is

$$\dot{\delta}_c = -\frac{1}{2}\dot{h}. \quad (15)$$

Here we note that the velocity perturbation for CDM is set as $\theta_c = 0$ so that we can fix the gauge freedom in the synchronous gauge. For baryon, we have

$$\dot{\delta}_b = -\theta_b - \frac{1}{2}\dot{h}, \quad \dot{\theta}_b = \mathcal{H}\theta_b + Rn_e\sigma_T(\theta_\gamma - \theta_b), \quad (16)$$

where σ_T is the cross section for the Thomson scattering and n_e is the number density of electron, and we also have defined $R \equiv 4\bar{\rho}_\gamma/(3\bar{\rho}_b)$. For photons, the equations are:

$$\dot{\delta}_\gamma = -\frac{4}{3}\theta_\gamma - \frac{2}{3}\dot{h}, \quad \dot{\theta}_\gamma = k^2\left(\frac{1}{4}\delta_\gamma - \sigma_\gamma\right) - an_e\sigma_T(\theta_\gamma - \theta_b). \quad (17)$$

Similarly, for neutrinos, the equations of motion are

$$\dot{\delta}_\nu = -\frac{4}{3}\theta_\nu - \frac{2}{3}\dot{h}, \quad \dot{\theta}_\nu = k^2\left(\frac{1}{4}\delta_\nu - \sigma_\nu\right). \quad (18)$$

Here we have omitted the equation for the anisotropic stress and higher multipole moments for photons and those for neutrinos since they are not so relevant to our discussion and we do not discuss in the following.

During the epoch deep in the radiation dominated era, the time scale of the Thomson scattering is much shorter than the Hubble expansion, which dampens anisotropic stress of photons and drives the velocity perturbations of baryon and photons the same. Thus in the above equations, we can set $\sigma_\gamma = 0$ and $\theta_b = \theta_\gamma$ in early times when the initial conditions are given. Furthermore, on superhorizon scales, the terms with velocity perturbations can

be regarded as smaller by a factor of $k^{\#4}$, which allows us to neglect those terms at leading order of k . Then we obtain the following relations at the leading order in $k\tau$:

$$\dot{h} = -2\dot{\delta}_c = -2\dot{\delta}_b = -\frac{3}{2}\dot{\delta}_\gamma, \quad (19)$$

which shows that the evolutions of δ_i follows that of h with some numerical factors except a constant term which can be determined by the initial condition for the perturbations.

On the other hand, inside the horizon, the evolutions of fluctuations are different from those on superhorizon scales. Although CDM holds the relation with the metric perturbation h with Eq. (15), on subhorizon scales where $k\tau \gg 1$, baryon and photons obey the following equations:

$$\ddot{\delta}_b + \mathcal{H}\dot{\delta}_b + c_s^2 k^2 \delta_b = -\frac{1}{2}\mathcal{H}\dot{h} - \frac{\ddot{h}}{2}, \quad (20)$$

$$\ddot{\delta}_\gamma + \frac{1}{3}k^2 \delta_\gamma = -\frac{2}{3}\ddot{h}. \quad (21)$$

Since inside the horizon, δ_c grows as $\delta_c \propto \ln a$ during radiation-dominated (RD) era and $\delta_c \propto a$ during matter-dominated (MD) era, the metric perturbation h also evolves as $\dot{h} \propto 1/a$ and $a^{1/2}$ during RD and MD eras, respectively. Since the scale factor can be given by the conformal time τ as $a \propto \tau$ and τ^2 during RD and MD eras, respectively, from Eqs. (20) and (21), δ_b and δ_γ show oscillatory behaviors with almost constant amplitudes except the epoch of the transition from RD to MD. As will be discussed shortly, these behaviors are the same for adiabatic and isocurvature modes except the phases of the oscillations due to the difference of the initial conditions of these modes which are given when the fluctuations enter the horizon.

Now we discuss the evolutions of density fluctuations for each mode by showing those of CDM, baryon and photons. We start with the adiabatic mode. To identify the adiabatic mode, it is convenient to introduce the gravitational (Newtonian) potentials ϕ and ψ which are defined as the metric perturbations in the conformal Newtonian gauge:

$$ds^2 = a^2(\tau) \left[-d\tau^2(1 + 2\phi) + (1 - 2\psi)\delta_{ij}dx^i dx^j \right]. \quad (22)$$

The metric perturbations h and η in the synchronous gauge can be related to ϕ and ψ as

$$\phi = \frac{1}{2k^2} \left[\ddot{h} + 6\ddot{\eta} + \mathcal{H}(\dot{h} + 6\dot{\eta}) \right], \quad \psi = \eta - \frac{\mathcal{H}}{2k^2}(\dot{h} + 6\dot{\eta}). \quad (23)$$

In the previous section, we have defined the primordial power spectrum for the adiabatic mode with the curvature perturbation ζ , which is related to ψ and ϕ as

$$\zeta = \psi + \frac{2}{3(1+w)} \left[\phi + \frac{\dot{\psi}}{\mathcal{H}} \right], \quad (24)$$

^{#4} This is not true in the neutrino density and velocity isocurvature modes [18], which we do not consider in this paper.

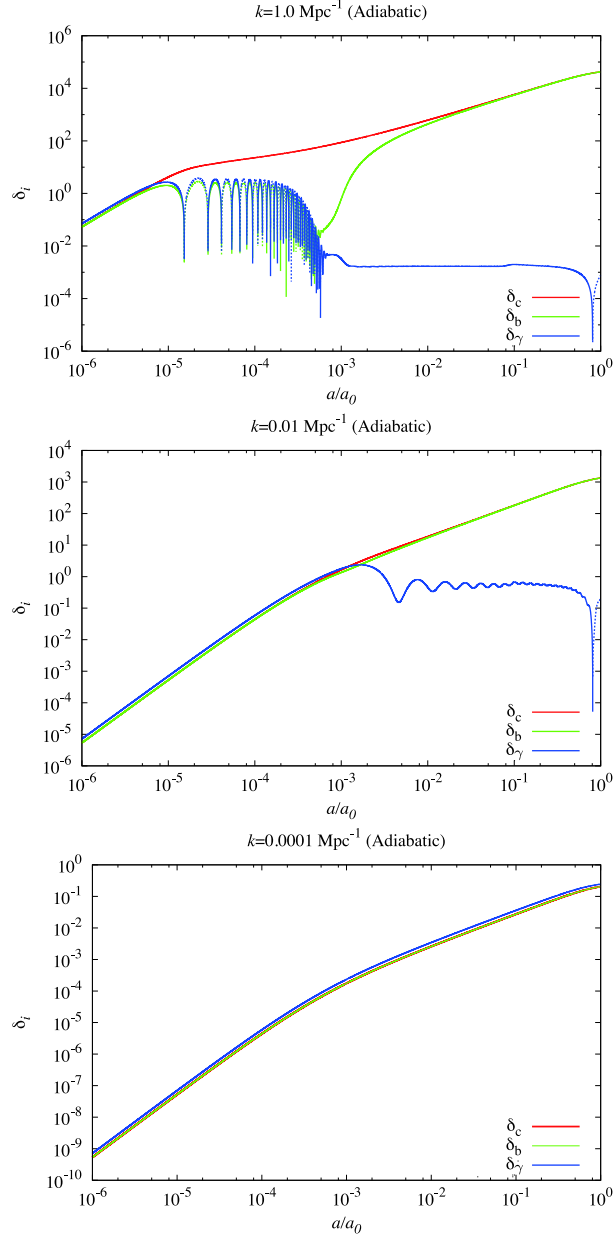


Figure 1: Evolutions of δ_c , δ_b and δ_γ for adiabatic mode in the synchronous gauge. Here we show those for $k = 1.0$ (top), 0.01 (middle) and 0.0001 Mpc^{-1} (bottom).

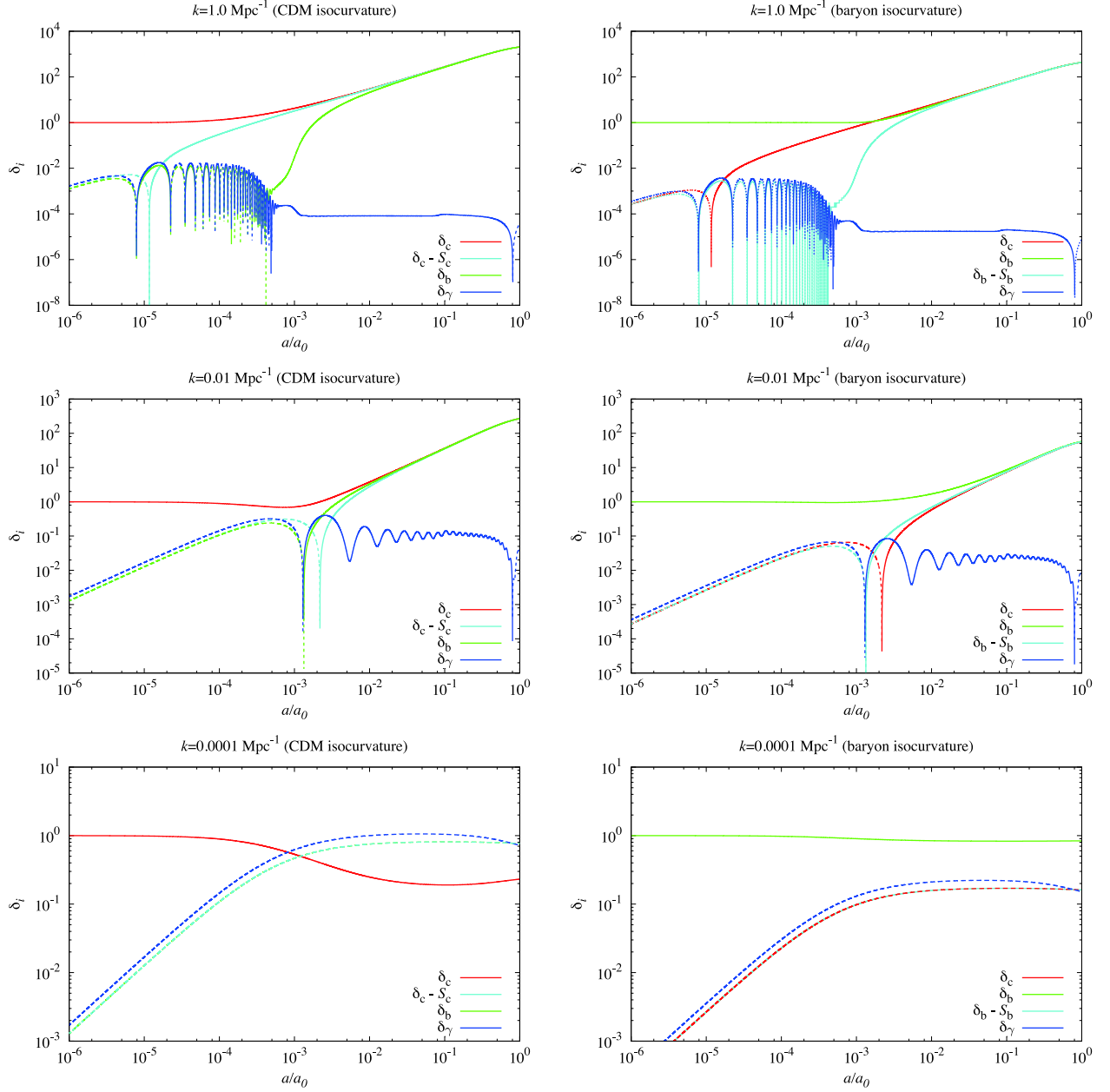


Figure 2: Evolutions of δ_c , δ_b and δ_γ for CDM isocurvature mode (left panel) and baryon one (right panel) in the synchronous gauge. Evolutions of $\delta_c - S_c$ and $\delta_c - S_b$ for CDM and baryon isocurvature modes respectively are also plotted. Here we show those for $k = 1.0$ (top), 0.01 (middle) and 0.0001 Mpc^{-1} (bottom).

where $w = \bar{P}/\bar{\rho}$ is the equation of state for the total component.

The adiabatic mode can be identified with a non-zero value of ζ for $\tau \rightarrow 0$, which leads to a solution on superhorizon scales as, at leading order in the series of $k\tau$ [18],

$$h/\zeta(0) = \frac{1}{2}k^2\tau^2, \quad (25)$$

$$\eta/\zeta(0) = 1 - \frac{5 + 4f_\nu}{12(15 + 4f_\nu)}k^2\tau^2, \quad (26)$$

$$\delta_c = \delta_b = \frac{3}{4}\delta_\gamma = \frac{3}{4}\delta_\nu = -\frac{1}{4}k^2\tau^2\zeta(0), \quad (27)$$

$$\theta_\gamma = \theta_b = -\frac{1}{36}k^4\tau^3\zeta(0), \quad (28)$$

$$\theta_\nu/\zeta(0) = -\frac{1}{36} \left[\frac{4f_\nu + 23}{4f_\nu + 15} \right] k^4\tau^3, \quad (29)$$

with the fraction of neutrinos in the energy density of radiations being denoted as $f_\nu = \frac{\Omega_\nu}{\Omega_\gamma + \Omega_\nu}$. Here the conformal time τ is normalized such that the scale factor is given by $a(\tau) = \tau + \tau^2$ with the normalization for a being $a_{\text{eq}} = 1/4$. Although our main focus in this section is the evolutions of density fluctuations in models with isocurvature modes, for reference, we show those in the adiabatic mode in Fig. 1. In the figure, cosmological parameters are taken as $\Omega_b h^2 (\equiv \omega_b) = 0.0227$, $\Omega_c h^2 (\equiv \omega_c) = 0.108$, $h = 0.724$ and $\tau_{\text{reion}} = 0.089$, where $\Omega_i = \rho_i(a_0)/\rho_{\text{crit}}$ is density parameter for a species i , h is the Hubble parameter and τ_{reion} is the optical depth for reionization. Unless otherwise stated, we assume these values in this paper.

Next we look at the evolutions of density perturbations in the CDM isocurvature mode. This mode can be identified with a non-zero value of δ_c at $\tau \rightarrow 0$, which we denote as S_c . Notice that even in this mode, the evolutions of δ_i and h follow Eq. (19). Then the superhorizon solution in early times can be given by [18]

$$h/S_c = 4\Omega_c\tau - 6\Omega_c\tau^2, \quad (30)$$

$$\eta/S_c = -\frac{2}{3}\Omega_c\tau + \Omega_c\tau^2, \quad (31)$$

$$\delta_c/S_c = 1 - 2\Omega_c\tau + 3\Omega_c\tau^2, \quad (32)$$

$$\delta_b = \frac{3}{4}\delta_\gamma = \frac{3}{4}\delta_\nu = (-2\Omega_c\tau + 3\Omega_c\tau^2)S_c, \quad (33)$$

$$\theta_\gamma = \theta_b = \theta_\nu = -\frac{1}{3}\Omega_c k^2\tau^2 S_c. \quad (34)$$

Notice that the metric perturbations h and η are induced by the existence of the initial isocurvature fluctuations. Importantly, once the metric perturbations are induced, density fluctuations are also generated through gravity, which satisfy the adiabatic condition as for those of the adiabatic mode. Thus the superhorizon solution of δ_c for the CDM isocurvature mode has the structure of the form:

$$\delta_c = (\text{initial fluctuations}) + (\text{induced from metric perturbations}). \quad (35)$$

In the left panels of Fig. 2, we show the evolutions of δ_c , δ_b , δ_γ as well as $\delta_c - S_c$ which corresponds to the part induced by the metric perturbations in this mode.

On the other hand, the baryon isocurvature mode can be identified as a mode where δ_b does not vanish in the early times. The superhorizon solution in this mode is

$$h/S_b = 4\Omega_b\tau - 6\Omega_b\tau^2, \quad (36)$$

$$\eta/S_b = -\frac{2}{3}\Omega_b\tau + \Omega_b\tau^2, \quad (37)$$

$$\delta_b/S_b = 1 - 2\Omega_b\tau + 3\Omega_b\tau^2, \quad (38)$$

$$\delta_c = \frac{3}{4}\delta_\gamma = \frac{3}{4}\delta_\nu = (-2\Omega_b\tau + 3\Omega_b\tau^2)S_b, \quad (39)$$

$$\theta_\gamma = \theta_b = \theta_\nu = -\frac{1}{3}\Omega_b k^2 \tau^2 S_b, \quad (40)$$

where the initial value of δ_b is denoted as S_b . The superhorizon solution for baryon isocurvature mode above can be obtained by just replacing Ω_c in those for the CDM one with Ω_b (and S_c with S_b) except that δ_b and δ_c are replaced with each other. Thus as far as δ_γ is concerned, its evolutions in CDM and baryon isocurvature modes are the same besides some overall factors such as Ω_c and Ω_b originating from the amount of CDM and baryon (see Fig. 2).

So far we have seen that the initial, superhorizon solutions of all perturbed quantities other than δ_c and δ_b differ only by an overall constant between the CDM and baryon isocurvature modes. In fact, this is also true for all subsequent times, which was also noted in [24] previously. Here we discuss this issue in some details.

First of all, the superhorizon (initial) solutions of all perturbation quantities other than δ_c and δ_b are determined by the initial total matter isocurvature perturbation $S_m = f_c S_c + f_b S_b$, not by S_c and S_b separately (here $f_c = \Omega_c/\Omega_m$, $f_b = \Omega_b/\Omega_m$ and $\Omega_m = \Omega_c + \Omega_b$), which can be noticed by rewriting the superhorizon solutions with S_m :

$$h = [4\Omega_m\tau - 6\Omega_m\tau^2] S_m, \quad (41)$$

$$\eta = \left[-\frac{2}{3}\Omega_m\tau + \Omega_m\tau^2\right] S_m, \quad (42)$$

$$\delta_\gamma = \delta_\nu = \left[-\frac{8}{3}\Omega_m\tau + 4\Omega_m\tau^2\right] S_m, \quad (43)$$

$$\theta_\gamma = \theta_b = \theta_\nu = -\frac{1}{3}\Omega_m k^2 \tau^2 S_m, \quad (44)$$

$$\delta_m = [1 - 2\Omega_m\tau + 3\Omega_m\tau^2] S_m, \quad (45)$$

where $\delta_m = f_c\delta_c + f_b\delta_b$. (Pure) CDM and baryon isocurvature modes correspond to the cases of $S_b = 0$ and $S_c = 0$, respectively. Secondly, the time derivatives of the perturbed quantities of any fluids are dependent on δ_c and δ_b only through the metric perturbations h and hence the matter perturbation δ_m (See Eqs. (15-18)). Therefore, as far as the value of S_m is fixed, regardless of the values of S_c and S_b , the subsequent time evolutions

of all perturbed quantities apart from δ_b and δ_c are the same. For instance, as can be seen (except for the overall normalization) in Fig. 2, the evolution of δ_γ is the same for the CDM and baryon isocurvature modes. This explains that models with the same S_m give identical CMB power spectra. Therefore, in the linear cosmological perturbation theory, the CDM and baryon isocurvature modes are in principle indistinguishable from observations of CMB. Furthermore, they also cannot be distinguished by observations of neither the metric nor the total matter perturbations.

Put in another way, the above can also be understood as follows. From a naive expectation, one may ask why δ_c and δ_b would affect the perturbation evolutions in the same way even though baryon couples to photons while CDM does not. The reason is twofold. First, photons and baryon couple via the elastic Thomson scattering and the momentum is just transferred between photons and baryons. Therefore the photon perturbations are affected by θ_b , but not by δ_b (See Eq. (17)). Second, both CDM and baryon are pressureless matter, thus the velocity perturbations of these fluids θ_c and θ_b are not generated from the density perturbations δ_c and δ_b (See Eq. (16)), which is not true for photons or neutrinos (See Eqs. (17) and (18)). These two facts explain that δ_b and δ_c affect the evolution of cosmological perturbations only through gravity in the same manner.

While the CDM and baryon isocurvature modes cannot be distinguished from the perturbations in the photon fluid nor the metric, the evolutions of δ_c and δ_b are different between these two modes as seen from Fig. 2. Although the evolutions of the induced parts of δ_c and δ_b (represented as $\delta_c - S_c$ and $\delta_b - S_b$ in Fig. 2) from the metric perturbations are also the same except some constant factor and retain the relation implied by Eq. (19), the initial nonzero fluctuations of δ_c and δ_b for CDM and baryon isocurvature modes should be superimposed, respectively, on those induced parts. Thus the evolutions of δ_c and δ_b are different, which gives a possibility of differentiating these modes. Although the difference between δ_c and δ_b becomes small on small scales since baryon density fluctuations catch up those of dark matter after the recombination and entering the horizon. However, on large scales, as seen from the bottom panels of Fig. 2, we can see some differences between δ_c and δ_b even at later epoch. Interestingly, we can in principle observe this difference by looking at 21 cm fluctuations which effectively probe the fluctuations of baryon. In the next section, we discuss this issue in some details.

3 CDM and baryon isocurvature fluctuations with 21 cm Survey

3.1 21 cm fluctuations

First we briefly summarize the fluctuations in redshifted 21 cm line emission. Even after recombination at $z \simeq 1090$, the photon and the hydrogen gas are still in kinetic equilibrium via the Compton scattering due to a small fraction of free electrons. At around a redshift $z \simeq 300$, the interaction becomes ineffective and thereafter the gas cools adiabatically. The

gas temperature T_{gas} scales as a^{-2} , while the photon temperature T_γ scales as a^{-1} . At first, the 21 cm spin flip driven by the atomic collision is so frequent that the spin temperature T_s ^{#5} tracks T_{gas} . As gas cools faster than CMB, the atomic collision subsequently becomes less effective and the interaction with the abundant CMB photons in turn dominates. Then T_s catches up with T_γ until the formation of first objects, which is supposed to take place at $z \lesssim 30$. Since T_s remains lower than T_γ throughout this ‘dark age’ at redshifts $30 \lesssim z \lesssim 300$, the redshifted 21 cm line intensity is observed as an absorption compared with the CMB intensity at the microwave band [25].

The unperturbed brightness temperature of 21 cm line observed now at an observed frequency ν can be calculated by [25, 26]

$$\bar{T}_b(\nu) = \left[(1 - e^{-\tau_{21\text{cm}}}) \frac{\bar{T}_s - \bar{T}_\gamma}{1 + z} \right] (z_\nu) \quad (46)$$

where z_ν is the redshift of the 21 cm transition at the frequency ν , i.e. $(1 + z_\nu) = \nu_0/\nu$, with the frequency of 21 cm emission being denoted by $\nu_0 \simeq 1.4$ GHz. $\tau_{21\text{cm}}(z)$ is the optical depth of 21 cm, which can be given by

$$\begin{aligned} \tau_{21\text{cm}}(z) &= \left[\frac{3A_{10}\bar{n}_{\text{HI}}}{16\nu_0^2\bar{T}_s(1+z)\mathcal{H}} \right] (z) \\ &= 1.081 \times 10^{-2} \bar{x}_H \left[\frac{\bar{T}_s}{\bar{T}_\gamma}(z) \right]^{-1} \left[\frac{\omega_b}{0.023} \right] \left[\frac{\omega_m}{0.13} \right]^{-1/2} \left[\frac{1+z}{10} \right]^{1/2}, \end{aligned} \quad (47)$$

where $A_{10} = 2.85 \times 10^{-15} \text{ s}^{-1}$ is the spontaneous emission coefficient, \bar{n}_{HI} is the number density of neutral hydrogen, x_{HI} is the neutral hydrogen fraction, and $\omega_m \equiv \omega_b + \omega_c$. In this paper we consider observations at redshifts $z_\nu \gtrsim 30$ so that complexities arising from nonlinear physics can be much reduced. In particular, we consistently set $\bar{x}_H = 1$ at these redshifts, adopting the standard assumption that the onset of the reionization occurs at latter epoch. Then $\bar{T}_b(\nu)$ in Eq. (46) can be given by

$$\bar{T}_b(\nu) = 29.50\text{mK} \left[\frac{\bar{T}_s - \bar{T}_\gamma}{\bar{T}_s}(z_\nu) \right] \left[\frac{\omega_b}{0.023} \right] \left[\frac{\omega_m}{0.13} \right]^{-1/2} \left[\frac{1+z_\nu}{10} \right]^{1/2}. \quad (48)$$

Now we turn our attention to the fluctuations in T_b . While there can be a number of sources generating the 21 cm brightness temperature fluctuations, the most dominant ones are as follows: (1) the monopole source arising from the density fluctuations of neutral hydrogen and relative temperature difference between the spin and CMB, (2) the Doppler redshift due to the peculiar velocity of neutral hydrogen gas against the observer. Taking into account these two effects, fluctuations in T_b at frequency ν observed at position \vec{r}_0 and conformal time τ_0 in a sight direction \hat{n} can be given by [27]

$$\Delta T_b(\nu, \hat{n}) = \bar{T}_b(\nu) e^{-\tau_{\text{reion}}} \left[\Delta n_{\text{HI}} + \frac{\bar{T}_\gamma}{\bar{T}_s - \bar{T}_\gamma} (\Delta T_s - \Delta T_\gamma) + \frac{\tau_{21\text{cm}}}{e^{\tau_{21\text{cm}}} - 1} \hat{n} \cdot \frac{d\vec{v}/d\tau}{\mathcal{H}} \right] (\vec{r}_\nu, \tau_\nu), \quad (49)$$

^{#5} T_s determines the number ratio of neutral hydrogens in the triplet and singlet states, $n_{\text{triplet}}/n_{\text{singlet}} = 3e^{-E_*/T_s}$, where E_* is the energy difference between the singlet and triplet states.

where $\Delta_X \equiv (X - \bar{X})/\bar{X}$ represents the fractional perturbation of a quantity X in the Newtonian gauge. Eq. (49) is formal solution from the line of sight integration, and the right hand side should be evaluated at position $\vec{r}_\nu = \vec{r}_0 + \hat{n}(\tau_0 - \tau_\nu)$ and time $\tau = \tau_\nu$, where τ_ν is the conformal time at z_ν . As shown in [27], in a redshift range $z \gtrsim 30$, other sources of 21 cm brightness temperature fluctuations are not very significant (at most percent-level at very large angular scales), as long as narrow redshift window functions are adopted. Therefore in the following, we adopt Eq. (49) as the theoretical prediction of observable 21 cm fluctuations.

The observed fluctuations in 21 cm intensity are determined by the fluctuations in the spin temperature ΔT_s , as well as $\Delta_{n_{\text{HI}}}$, Δ_{T_γ} and \vec{v} . Since the rates of the spin flip transition due to atom collisions and photon interaction are sufficiently high, the evolution of ΔT_s can well be determined by assuming equilibrium. For a comprehensive discussion for the evolution equations for ΔT_s and other fluctuations related for 21 cm fluctuations, we refer to [27].

3.2 3-dim power spectrum from 21 cm tomography observations

21 cm photons emitted at some redshift z now would be observed at a distinct frequency $\nu = \nu_0/(1+z)$. This allows us to perform tomographic reconstruction of 3-dim power spectrum of redshifted 21 cm fluctuations [25, 26, 28].

Let us consider a tomographic observation of 21 cm fluctuations around a fixed frequency ν and a direction \hat{n} in the sky. The observed frequency and sky position constitute a 3-dim space and we denote its coordinate as $(\delta\nu, \vec{\Theta})$. Once given a background cosmology, there is a one-to-one correspondence between $(\delta\nu, \vec{\Theta})$ and the coordinate of 3-dim real space $(r_\parallel, \vec{r}_\perp)$:

$$r_\parallel = y(z_\nu)\delta\nu, \quad \vec{r}_\perp = d_A(z_\nu)\vec{\Theta}, \quad (50)$$

where the subscripts \parallel and \perp represent the direction parallel and transverse to the line of sight, respectively. The conversion factors between $(\delta\nu, \vec{\Theta})$ and (r_\parallel, r_\perp) are given by

$$y(z) = \frac{(1+z)^2}{\nu_0 H(z)}, \quad (51)$$

$$d_A(z) = \int_0^z \frac{dz'}{H(z')}. \quad (52)$$

In particular, $d_A(z)$ is the comoving angular diameter distance. Then a Fourier dual of $(\delta\nu, \vec{\Theta})$, which we denote as $(u_\parallel, \vec{u}_\perp)$, can also be related to the wave vector $(k_\parallel, \vec{k}_\perp)$ via

$$k_\parallel = u_\parallel/y(z_\nu), \quad \vec{k}_\perp = \vec{u}_\perp/d_A(z_\nu). \quad (53)$$

From the formal solution Eq. (49), we obtain the power spectrum of 21 cm fluctuations observed at around frequency ν and sight direction \hat{n} in \vec{k} space

$$P_{\Delta T_b}(\vec{k}; \nu, \hat{n}) = \bar{I}_b^2 e^{-2\tau_{\text{reion}}} [P_{00}(k, z_\nu) - 2\mu^2 P_{01}(k, z_\nu) + \mu^4 P_{11}(k, z_\nu)], \quad (54)$$

where μ is the cosine of angle between \hat{n} and \vec{k} , i.e. $\mu = \hat{n} \cdot \vec{k}/k$. Here P_{00} , P_{11} , P_{01} are the power spectra of auto-correlations of monopole $\Delta_0 \equiv \Delta_{n\text{HI}} + \frac{\bar{T}_\gamma}{T_s - T_\gamma}(\Delta T_s - \Delta T_\gamma)$ and dipole moments $\Delta_1 \equiv \frac{\tau_{21\text{cm}}}{e^{\tau_{21\text{cm}} - 1}} \frac{kv}{\mathcal{H}}$ of the source and their cross-correlation, i.e.

$$\langle \Delta_0(\vec{k}, z) \Delta_0(\vec{k}', z) \rangle = P_{00}(k, z) (2\pi)^3 \delta^{(3)}(\vec{k} + \vec{k}'), \quad (55)$$

$$\langle \Delta_1(\vec{k}, z) \Delta_1(\vec{k}', z) \rangle = P_{11}(k, z) (2\pi)^3 \delta^{(3)}(\vec{k} + \vec{k}'), \quad (56)$$

$$\langle \Delta_0(\vec{k}, z) \Delta_1(\vec{k}', z) \rangle = P_{01}(k, z) (2\pi)^3 \delta^{(3)}(\vec{k} + \vec{k}'). \quad (57)$$

By performing a Fourier transformation of the two-point correlation function of the 21 cm fluctuations $\langle \Delta T_b(\vec{r}) \Delta T_b(\vec{r}') \rangle$, the power spectrum defined in the \vec{u} space, $P_{\Delta T_b}(\vec{u})$, can be related to one in the wave vector space via

$$P_{\Delta T_b}(\vec{u}, \nu) = \frac{1}{d_A^2(z_\nu) y(z_\nu)} P_{\Delta T_b}(\vec{k}, z_\nu). \quad (58)$$

Note that due to the Doppler effect, the power spectrum of 21 cm fluctuations $P_{\Delta T_b}(\vec{u})$ is not isotropic; it is instead a function of both u_\parallel and u_\perp or, equivalently, both k_\parallel and k_\perp .

In Fig. 3, we show the 21 cm power spectra for the cases with pure CDM and baryon isocurvature fluctuations. To calculate the power spectra for 21 cm fluctuations, we used `CAMB sources` [27]. For reference, we also show expected sensitivity from the Fast Fourier Transform Telescope (FFTT) which can probe the redshift $z > 30$ and is described in [29]. An explicit form of noise power spectrum $P_{\Delta T_b}^{\text{noise}}(\vec{u})$ is given in Eq. (61) and some detailed descriptions will be given in the next subsection.

Although any pure isocurvature modes are already excluded by current observations of CMB, we show pure isocurvature spectra to see to what extent we can tell the difference between CDM and baryon isocurvature modes. In the top panels of Fig. 3, we show power spectra for the case with $n_s^{(\text{CDMiso})} = n_s^{(\text{biso})} = 1$. The amplitude of primordial fluctuations for CDM mode is fixed as $\mathcal{P}_{S_c}(k_0) = 2.41 \times 10^{-9}$ at $k = 0.002 \text{ Mpc}^{-1}$. For the baryon mode, the amplitude is assumed to give exactly the same CMB angular power spectrum as that for CDM (i.e., the initial amplitude is $(\Omega_c/\Omega_b)^2$ times large as that for CDM mode). The bottom panels show the case of very blue-tilted spectra with $n_s^{(\text{CDMiso})} = n_s^{(\text{biso})} = 3$. Although the spectral indices of this kind of value seem somewhat too large, it has been claimed that blue-tilted (CDM/baryon) isocurvature spectrum may be favored by observations [22, 30–34]^{#6}. In addition, some axion model producing very blue-tilted spectrum has been discussed [12], and in their model, the spectral index for the CDM isocurvature perturbations can be as large as 4, depending on parameters. In light of these, it would be interesting to investigate isocurvature models with very blue-tilted spectra.

As seen from Fig. 3, the survey of 21 cm fluctuations gives different power spectra for CDM and baryon isocurvature fluctuations, which enables us to discriminate these modes.

^{#6} A recent analysis puts a constraint on the spectral index as $n_s^{(\text{CDMiso})} = 2.246_{-0.428}^{+0.494}$ [34].

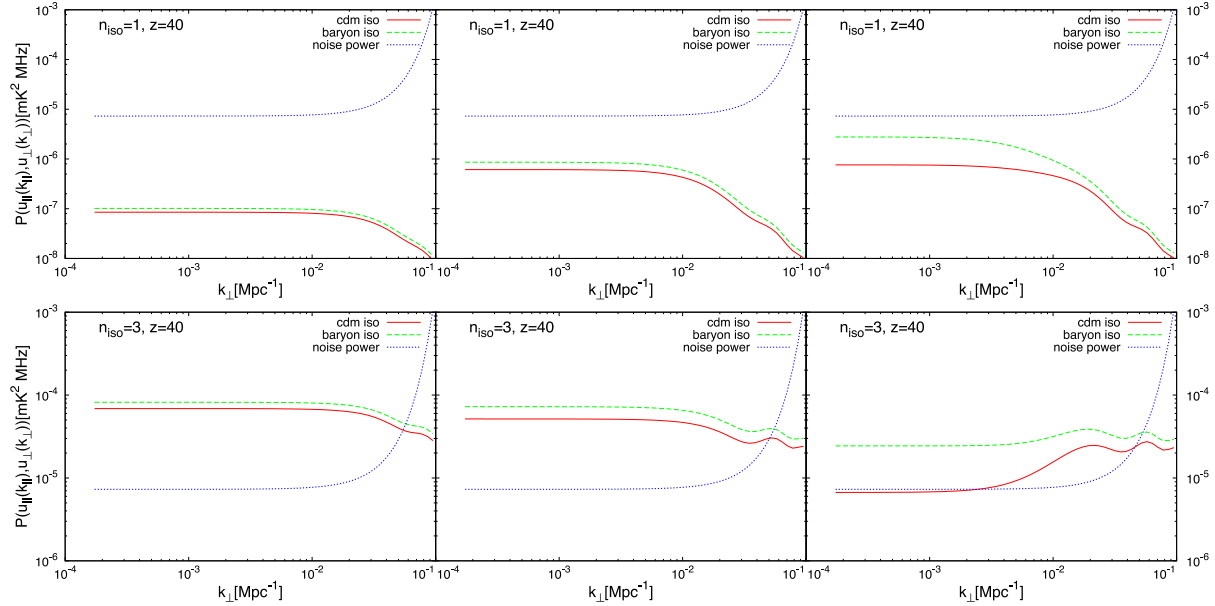


Figure 3: 21 cm power spectra $P_{\Delta T_b}(u_{\parallel}, u_{\perp})$ at $z = 40$ for the cases with pure CDM (solid red line) and baryon (dashed green line) isocurvature modes. The spectral indices are assumed as $n_s^{(\text{CDMiso})} = n_s^{(\text{biso})} = 1$ (top) and $n_s^{(\text{CDMiso})} = n_s^{(\text{biso})} = 3$ (bottom). In each panel, power spectra are shown as function of k_{\perp} with k_{\parallel} being fixed. From left to right, u_{\parallel} is fixed to 0.22MHz^{-1} , 0.72MHz^{-1} and 2.3MHz^{-1} , which respectively correspond to $k_{\parallel} \simeq 5.4 \times 10^{-3} \text{Mpc}^{-1}$, $1.7 \times 10^{-2} \text{Mpc}^{-1}$ and $5.6 \times 10^{-2} \text{Mpc}^{-1}$. The size of the baryon isocurvature mode is chosen such that the baryon isocurvature mode gives the same CMB power spectrum with the CDM one. We also show the FFTT noise power spectra (dotted blue line).

However, when the primordial spectra are assumed to be scale-invariant (top panels), the signals are too weak compared with sensitivities of observations. On the other hand, for the case with $n_s^{(\text{CDMiso})} = n_s^{(\text{biso})} = 3$ (bottom panels), the amplitudes become large and difference in power spectra can be larger than the noise power. So we expect that these kinds of isocurvature modes can be differentiated with the 21 cm survey of FFTT.

In fact, even when we consider a realistic case where CDM/baryon isocurvature fluctuations give subdominant contributions to the total (almost adiabatic) spectrum allowed by current observations, we can still probe the difference between CDM and baryon isocurvature modes. In Fig. 4, we show the 21 cm spectra for $(r_c, r_b) = (0.1, 0)$ (red line) and $(r_c, r_b) = (0, 0.1 \times (\Omega_c/\Omega_b)^2)$ (green line). Contributions from the adiabatic perturbations are also included here. The choice of the value of r_b for the latter case is made so that these two cases give the indistinguishable CMB angular power spectra. In the figure, we also show the expected error in measuring power spectrum $\delta P_{\Delta T_b}(\vec{u})$, as well as that for the noise $P_{\Delta T_b}^{\text{noise}}(\vec{u})$. An explicit expression of $\delta P_{\Delta T_b}(\vec{u})$ is given in Eq. (64). While the noise power spectrum is estimated from the detector noise, error accounts for both the cosmic variance (assuming a vanilla model with the WMAP 7yr mean parameters [1]) and survey setups. The figure indicates that these two cases can be differentiated with the FFTT survey. To see this issue more quantitatively, in particular, to what extent we can probe the difference with a future 21 cm tomography observation such as FFTT, we make a forecast by adopting the Fisher information matrix analysis in the next section. In closing this section, we also note that the difference between the two isocurvature modes are more prominent at higher redshifts. This reflects the fact that the density perturbation in baryon catches up with one in CDM as redshift decreases, as we mentioned in the previous section.

3.3 Discriminating CDM and baryon isocurvature fluctuations with future 21 cm survey

Now we make a quantitative discussion about the possibility of discriminating CDM and baryon isocurvature modes with future observations of 21 cm fluctuations. For this purpose, we assume FFTT [29] for 21 cm survey. Although 21 cm surveys can probe the difference between CDM and baryon isocurvature modes, regarding other cosmological parameters, CMB observations are much more powerful. Thus we also include a future CMB observation, for which we assume the specification of CMBpol [35] in the Fisher matrix analysis.

Before presenting our results, here we briefly describe the formalism of the Fisher matrix analysis. Since we use expected measurements of CMB and 21 cm survey, the Fisher matrix F_{ij} can be given by the sum of two contributions:

$$F_{ij} = F_{ij}^{(\text{CMB})} + F_{ij}^{(21\text{cm})}, \quad (59)$$

where indices i, j represent cosmological parameters and $F_{ij}^{(\text{CMB})}$ and $F_{ij}^{(21\text{cm})}$ respectively indicate the contributions from CMB and 21 cm observations. We analyze a forecast in a 9

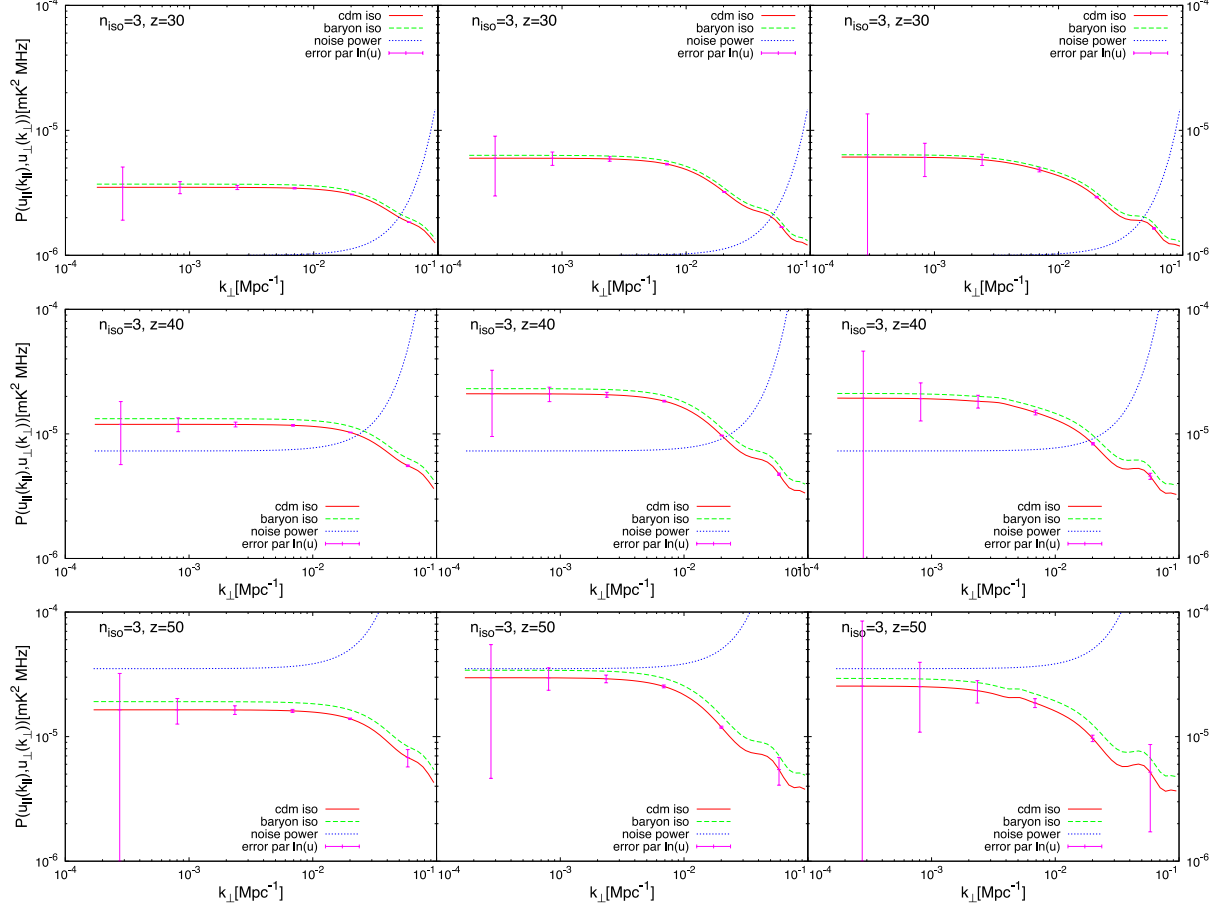


Figure 4: 21 cm power spectra $P_{\Delta T_b}(u_{\parallel}, u_{\perp})$ from the mixture of adiabatic and uncorrelated matter isocurvature perturbations. From top to bottom, we show power spectra at $z = 30$, 40 and 50 in order. In each panel, power spectra are shown as a function of k_{\perp} , for a fixed k_{\parallel} . From left to right, u_{\parallel} is fixed to 0.22MHz^{-1} , 0.72MHz^{-1} and 2.3MHz^{-1} , which respectively correspond to $k_{\parallel} \simeq 5.4 \times 10^{-3} \text{Mpc}^{-1}$, $1.7 \times 10^{-2} \text{Mpc}^{-1}$ and $5.6 \times 10^{-2} \text{Mpc}^{-1}$. Shown are power spectra for the cases with $(r_c, r_b) = (0.1, 0)$ (dashed green line) and $(r_c, r_b) = (0, 0.1 \times (\Omega_c/\Omega_b)^2)$ (dotted blue line). The spectral indices for the isocurvature fluctuations are assumed as $n_s^{(\text{CDMiso})} = n_s^{(\text{biso})} = 3$. Notice that these two cases give completely the same CMB power spectrum. We also show the FFTT noise power spectra (dotted blue line) and expected errors in measuring 21 cm power spectrum (magenta bar). Errors are estimated adopting a pixelization, which is logarithmically uniform in $(u_{\parallel}, u_{\perp})$ with widths $\Delta \ln u_{\parallel} \simeq \Delta \ln u_{\perp} \simeq 1$.

Frequency (GHz)	beam FWHM (arcmin)	ΔT (μK arcmin)
45	17	5.85
70	11	2.96
100	8	2.29
150	5	2.21
220	3.5	3.39

Table 1: Specifications for the mid-cost (EPIC-2m) CMBpol mission used in the analysis. For polarization, ΔT is reduced by the factor of $\sqrt{2}$. We have excluded the highest and lowest frequency bands (30 GHz and 340 GHz) for a realistic foreground removal.

dimensional parameter space $(\omega_c, \omega_b, h, n_s, \tau_{\text{reion}}, n_s, A_s, r_c, r_b, n_s^{(\text{CDMiso})})$. The definitions of the parameters here are already given in Section 2.2 except A_s , the amplitude of primordial fluctuations at the reference scale $k = 0.002 \text{ Mpc}^{-1}$. Here we assume that the spectral index for baryon isocurvature mode is the same as that for CDM one, i.e., $n_s^{(\text{biso})} = n_s^{(\text{CDMiso})}$ is adopted in the analysis.

For the Fisher matrix for CMB $F_{ij}^{(\text{CMB})}$, we follow the method of [36] and assume the projected CMBpol mission [35]. More specifically, we use the specifications for the mid-cost (EPIC-2m) mission, which is given in Table 1.

The Fisher matrix from a 21 cm tomography survey can be given by [37, 38],

$$F_{ij}^{(21\text{cm})} = \int \frac{d^3u}{(2\pi)^3} \frac{V_\Theta}{P_{\Delta T_b}^{\text{tot}}(\vec{u})^2} \left(\frac{\partial P_{\Delta T_b}(\vec{u})}{\partial \lambda_i} \right) \left(\frac{\partial P_{\Delta T_b}(\vec{u})}{\partial \lambda_j} \right), \quad (60)$$

where λ_i is the i -th cosmological parameter and $P_{\Delta T_b}^{\text{tot}}(\vec{u})$ is the power spectrum of the total observed 21 cm fluctuations, which is the sum of the signal $P_{\Delta T_b}(\vec{u})$ and the noise power spectra $P_{\Delta T_b}^{\text{noise}}(\vec{u})$, i.e. $P_{\Delta T_b}^{\text{tot}}(\vec{u}) = P_{\Delta T_b}(\vec{u}) + P_{\Delta T_b}^{\text{noise}}(\vec{u})$. Here $V_\Theta = \Omega_{\text{FoV}} B$ is the survey volume in Θ space, where Ω_{FoV} and B are the solid angle in the field of view and the frequency band width, respectively. In the analysis, we set $\Omega_{\text{FoV}} = \pi$ and $B = 8 \text{ MHz}$, regardless of observed frequencies.

Noise power spectrum of FFTT can be given by [29]

$$P_{\Delta T_b}^{\text{noise}}(\vec{u}) = \frac{4\pi f_{\text{sky}} \lambda_\nu^2 T_{\text{sys}}^2}{A \Omega_{\text{FoV}} f_{\text{cover}} t_{\text{obs}}} W(\vec{u}_\perp)^{-2}. \quad (61)$$

Here f_{sky} is the observed sky fraction, λ_ν is the observed radio wave length, T_{sys} is the system temperature, A is the telescope area, and f_{cover} is the fraction of are covered by the array. In the analysis, we take $f_{\text{cover}} = f_{\text{sky}} = 1$, $A = 20 \text{ km}^2$ and $t_{\text{obs}} = 1 \text{ yr}$. $W(\vec{u}_\perp)$ is the beam response function, which in principle depends on the shape of the telescope. In the analysis, we assume a symmetric Gaussian beam and we take

$$W(\vec{u}_\perp) = \exp \left[-\frac{\lambda_\nu^2}{A} u_\perp^2 \right]. \quad (62)$$

Since both $P_{\Delta T_b}(\vec{u})$ and $P_{\Delta T_b}^{\text{noise}}(\vec{u})$ do not depend on the azimuthal direction in \vec{u} -space, we integrate the right hand side in Eq. (60) over this direction. In addition, we pixelize the \vec{u} space with widths Δu_{\parallel} and Δu_{\perp} in the line of sight and transverse directions, respectively. Then Eq. (60) can be approximated as

$$F_{ij}^{(21\text{cm})} \simeq \sum_{\text{pixels}} \frac{1}{\delta P_{\Delta T_b}(\vec{u})^2} \left(\frac{\partial P_{\Delta T_b}(\vec{u})}{\partial \lambda_i} \right) \left(\frac{\partial P_{\Delta T_b}(\vec{u})}{\partial \lambda_j} \right), \quad (63)$$

where $\delta P_{\Delta T_b}(\vec{u})$ is the error in power spectrum par pixel, which can be given by

$$\delta P_{\Delta T_b}(\vec{u}) = \sqrt{\frac{(2\pi)^2}{\Delta u_{\parallel} u_{\perp} \Delta u_{\perp} V_{\Theta}}} P_{\Delta T_b}^{\text{tot}}(\vec{u}). \quad (64)$$

Removal of foregrounds is one of the primary challenges in future observation of cosmological 21 cm fluctuations. We assume foregrounds are highly smooth in the frequency space, and can be removed to sufficient accuracy at $|u_{\parallel}| \geq 1/B$, where we assume $T_{\text{sys}} = 200\text{K}[(1+z)/10]^{2.6}$ is dominated by the sky temperature due to the Galactic synchrotron emission. Note that this choice of lowest $|u_{\parallel}|$ hardly affects our results, as we focus on a blue-tilted power spectra of isocurvature perturbations. In addition, we also exclude modes $k > k_{\text{max}} = 0.1 \text{ Mpc}^{-1}$ in the analysis, in order to neglect effects of the nonlinear evolution of matter perturbations.

In Fig. 5, we show projected constraints for r_c and r_b from CMBpol alone (solid red contours) and CMBpol+FFTT (shared regions). Regarding the observed redshifts of FFTT survey, we analyzed four different combinations: $z = 30$ (top left), $z = 40$ (top right), $z = 50$ (bottom left) and all these redshifts combined (bottom right). Here the fiducial values are assumed as $r_c = 0.1$ and $r_b = 0$ and $n_s^{(\text{CDMiso})} = n_s^{(\text{biso})} = 3$. Other cosmological parameters are assumed as those given in the previous section. Since CMB alone cannot in principle make a distinction between CDM and baryon isocurvature models, the constraint from CMBpol alone is completely degenerate along the line which gives the same amount of isocurvature fluctuations in term of matter:

$$\left(\frac{\Omega_c}{\Omega_m} \right)^2 r_c + \left(\frac{\Omega_b}{\Omega_m} \right)^2 r_b = C, \quad (65)$$

with $C = 0.1 \times (\Omega_c/\Omega_m)^2$. However, as one can see from the figure, by including 21 cm surveys, the degeneracy can be removed, which means that we can see the difference between CDM and baryon isocurvature modes with 21 cm fluctuation surveys, in particular, when isocurvature modes have very blue-tilted spectra such as $n_s^{(\text{CDMiso})} = n_s^{(\text{biso})} = 3$.

As discussed in the previous section, the difference between δ_c and δ_b is more prominent at higher redshifts. On the other hand, observational sensitivity is better for lower redshifts. For a fixed band width B and a maximum wave number for the linear perturbation evolution k_{max} , the increase in the signal overwhelms the increase in noise and the most stringent constraint is obtained at the highest redshift $z = 50$.

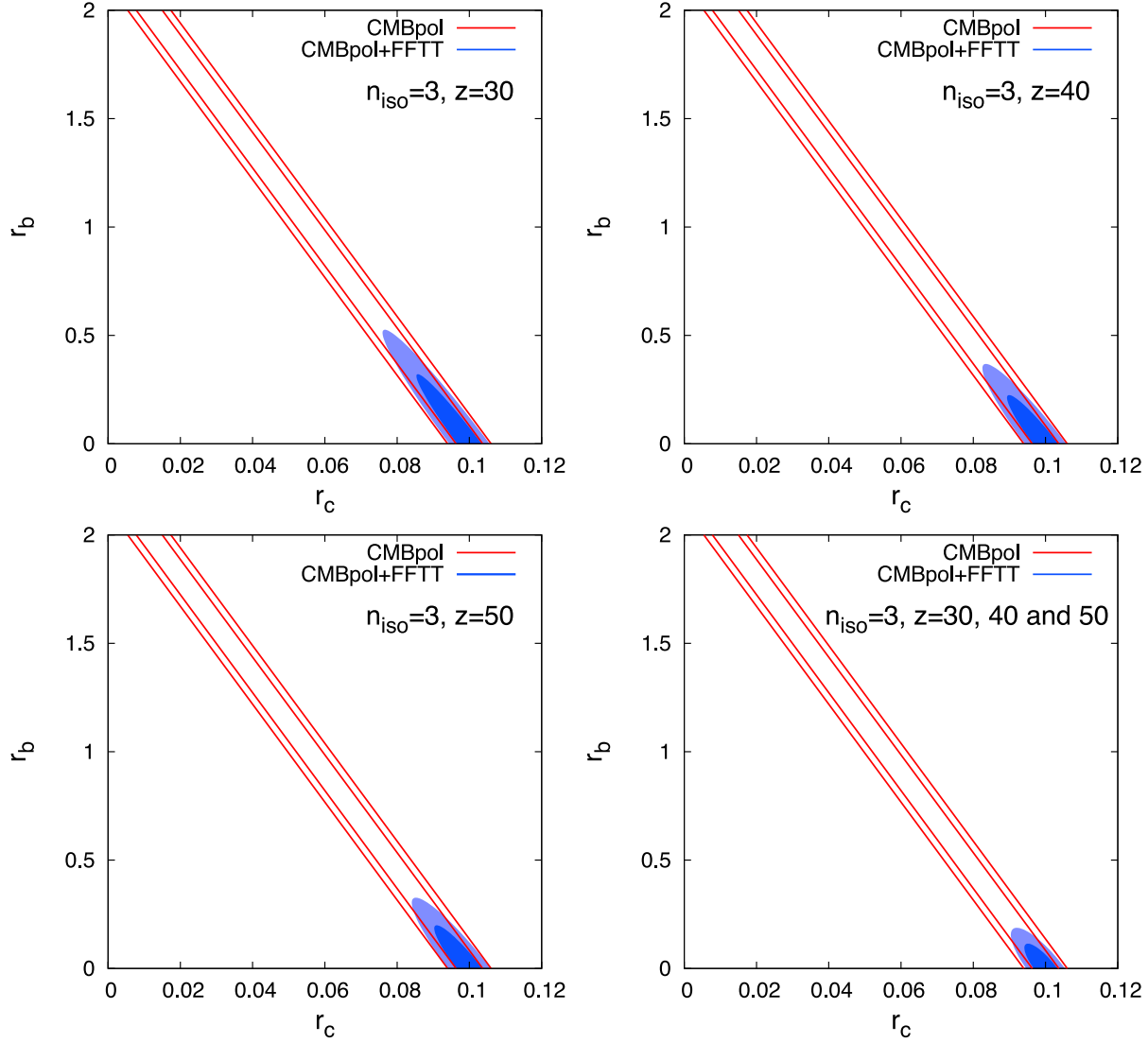


Figure 5: Expected 1σ and 2σ constraints on r_c and r_b from CMBpol alone (red contours) and CMBpol+FFTT (shaded regions). As for FFTT, we show constraints from different combinations of observed redshifts in separate panels; $z = 30$ (top left), $z = 40$ (top right), $z = 50$ (bottom left) and all of these redshifts $z = 30, 40$ and 50 (bottom right). The fiducial values are assumed as $(r_c, r_b) = (0.1, 0)$ and $n_s^{(\text{CDMiso})} = n_s^{(\text{biso})} = 3$.

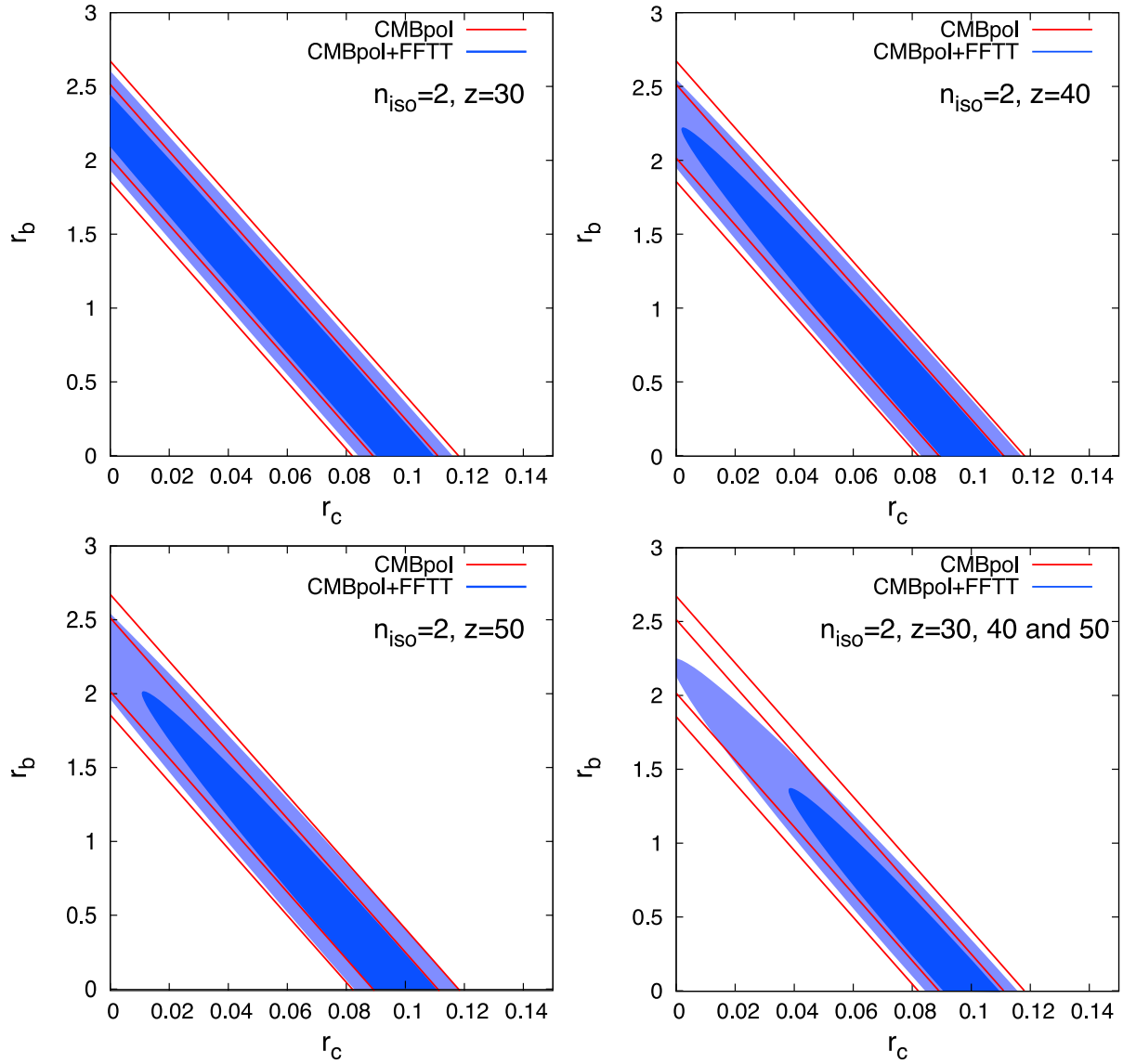


Figure 6: Same as in Fig. 5 but for $n_s^{(\text{CDMiso})} = n_s^{(\text{biso})} = 2$.

We also note that the constraint from the combination of three redshifts $z = 30, 40$ and 50 is at least twice as stringent as one from a single redshift $z = 50$. This suggests that a combination of different redshifts offers to some extent a synergy in discriminating the CDM and baryon isocurvature perturbations. This comes from the fact that parameter degeneracies between r_c or r_b and other cosmological parameters more or less differ at different redshifts. By combining observations at different redshifts, parameter degeneracies are partially removed and this gives severer constraints on r_c and r_b . Otherwise, the constraint from the combination of three redshifts would be at most as $\sqrt{3}$ times tighter as one from $z = 50$, which is the most stringent if a single redshift is observed.

Finally we comment on the dependence of constraints on the spectral indices of primordial isocurvature power spectra. In Fig. 6, we show constraints in the r_c - r_b plane for the case of $n_s^{(\text{CDMiso})} = n_s^{(\text{biso})} = 2$. As can be expected from the discussion in the previous section, constraints on r_c and r_b significantly degrade as the spectral indices become smaller. For the $n_s^{(\text{CDMiso})} = n_s^{(\text{biso})} = 2$, we may marginally discriminate the CDM and baryon isocurvature perturbations for a fiducial model $(r_c, r_b) = (0.1, 0)$. The significance is at around 1σ level from an observation at single redshift $z = 50$. By combining observations at all redshifts, the significance can be improved to around 2σ level. However, note that to what extent we can discriminate the CDM and baryon isocurvature perturbations depends on the maximum wave number for linear evolution. While we adopted a fixed $k_{\text{max}} = 0.1 \text{ Mpc}^{-1}$ at any observed redshifts, the use of larger k_{max} may be allowed as redshift becomes higher, which may offer more stringent constraints on r_c and r_b . On the other hand, for the case of $n_s^{(\text{CDMiso})} = n_s^{(\text{biso})} = 1$ we found FFTT does not improve constraints on r_c and r_b from CMBpol alone regardless of observed redshifts. This is what we expect from the top panels in Fig. 3. Thus the CDM and baryon isocurvature perturbations would be hardly distinguished if their power spectra are nearly scale invariant.

4 Summary

In this paper, we discussed a possibility of differentiating CDM and baryon isocurvature fluctuations with 21 cm survey. As is well-known, by using CMB observations, we cannot in principle see the difference between those modes although they can give a severe constraint on the sum of the size (fraction) of such isocurvature modes. However, once it is confirmed that CDM/baryon isocurvature perturbation should contribute to density fluctuations in the Universe even if the size is small, it would be very important to differentiate those modes since they can give invaluable information on the nature of dark matter/generation mechanism of baryon asymmetry of the Universe.

We showed that 21 cm fluctuation survey, which effectively probes density fluctuations of baryon, can in principle differentiate CDM and baryon isocurvature modes as shown in Figs. 3 and 4. To see this issue in some quantitative manner, we made a Fisher matrix analysis and discussed to what extent 21 cm survey can remove the complete degeneracy between the fractions of CDM and baryon isocurvature modes which resides in CMB. When

isocurvature fluctuations have scale-invariant primordial spectra, it seems very difficult to see the difference even with the FFT telescope. However, if isocurvature modes have very blue-tilted spectra, which is claimed to be favored by observations [22, 30–34], and is predicted in some axion model [12], it would be possible to distinguish CDM and baryon isocurvature modes, which we have explicitly shown in Fig. 5.

The adiabaticity of density fluctuations can give important information on various aspects of the Universe. In particular, in light that CDM/baryon isocurvature fluctuations might be generated in well-motivated scenarios of CDM and baryogenesis like axion models and Affleck-Dine baryogenesis, the differentiation of these two modes, which has been shown to be possible by using 21 cm fluctuation survey in this paper, may well give important implications for understanding the nature of CDM and baryogenesis scenario.

Acknowledgments

T. S. would like to thank the Japan Society for the Promotion of Science for financial support. This work is supported by Grant-in-Aid for Scientific research from the Ministry of Education, Science, Sports, and Culture, Japan, Nos. 14102004 (M.K.) and 21111006 (M.K.) and 19740145 (T.T.), and also by World Premier International Research Center Initiative (WPI Initiative), MEXT, Japan.

References

- [1] E. Komatsu *et al.* [WMAP Collaboration], *Astrophys. J. Suppl.* **192**, 18 (2011) [arXiv:1001.4538 [astro-ph.CO]].
- [2] M. Axenides, R. H. Brandenberger, M. S. Turner, *Phys. Lett.* **B126**, 178 (1983).
- [3] D. Seckel, M. S. Turner, *Phys. Rev.* **D32**, 3178 (1985).
- [4] A. D. Linde, *Phys. Lett.* **B158**, 375-380 (1985).
- [5] A. D. Linde, D. H. Lyth, *Phys. Lett.* **B246**, 353-358 (1990).
- [6] M. S. Turner, F. Wilczek, *Phys. Rev. Lett.* **66**, 5 (1991).
- [7] A. D. Linde, *Phys. Lett.* **B259**, 38 (1991).
- [8] D. H. Lyth, *Phys. Rev.* **D45**, 3394 (1992).
- [9] K. Enqvist and J. McDonald, *Phys. Rev. Lett.* **83**, 2510 (1999) [arXiv:hep-ph/9811412].
- [10] K. Enqvist, J. McDonald, *Phys. Rev.* **D62**, 043502 (2000) [hep-ph/9912478].

- [11] M. Kawasaki and F. Takahashi, Phys. Lett. B **516**, 388 (2001) [arXiv:hep-ph/0105134].
- [12] S. Kasuya, M. Kawasaki, Phys. Rev. **D80**, 023516 (2009) [arXiv:0904.3800 [astro-ph.CO]].
- [13] K. Enqvist, M. S. Sloth, Nucl. Phys. **B626**, 395 (2002) [hep-ph/0109214].
- [14] D. H. Lyth, D. Wands, Phys. Lett. **B524**, 5 (2002) [hep-ph/0110002].
- [15] T. Moroi and T. Takahashi, Phys. Lett. B **522**, 215 (2001) [Erratum-ibid. B **539**, 303 (2002)] [arXiv:hep-ph/0110096].
- [16] T. Moroi and T. Takahashi, Phys. Rev. D **66**, 063501 (2002) [arXiv:hep-ph/0206026].
- [17] D. H. Lyth and D. Wands, Phys. Rev. D **68**, 103516 (2003) [arXiv:astro-ph/0306500].
- [18] M. Bucher, K. Moodley, N. Turok, Phys. Rev. **D62**, 083508 (2000) [astro-ph/9904231].
- [19] R. Barkana and A. Loeb, Mon. Not. Roy. Astron. Soc. Lett. **363**, L36 (2005) [arXiv:astro-ph/0502083].
- [20] C. Gordon and J. R. Pritchard, Phys. Rev. D **80**, 063535 (2009) [arXiv:0907.5400 [astro-ph.CO]].
- [21] D. Grin, O. Dore and M. Kamionkowski, arXiv:1107.5047 [astro-ph.CO].
- [22] R. Bean, J. Dunkley and E. Pierpaoli, Phys. Rev. D **74**, 063503 (2006) [arXiv:astro-ph/0606685].
- [23] C. P. Ma and E. Bertschinger, Astrophys. J. **455**, 7 (1995) [arXiv:astro-ph/9506072].
- [24] C. Gordon and A. Lewis, Phys. Rev. D **67**, 123513 (2003) [arXiv:astro-ph/0212248].
- [25] D. Scott and M. J. Rees, Mon. Not. Roy. Astron. Soc. **247**, 510 (1990).
- [26] P. Madau, A. Meiksin and M. J. Rees, Astrophys. J. **475**, 429 (1997) [arXiv:astro-ph/9608010].
- [27] A. Lewis and A. Challinor, Phys. Rev. D **76**, 083005 (2007) [arXiv:astro-ph/0702600].
- [28] A. Kumar, T. Padmanabhan and K. Subramanian, Mon. Not. Roy. Astron. Soc. **272**, 544 (1995).
- [29] M. Tegmark and M. Zaldarriaga, Phys. Rev. D **79**, 083530 (2009) [arXiv:0805.4414 [astro-ph]].

- [30] R. Keskitalo, H. Kurki-Suonio, V. Muhonen and J. Valiviita, JCAP **0709**, 008 (2007) [arXiv:astro-ph/0611917].
- [31] M. Beltran, J. Garcia-Bellido, J. Lesgourgues and A. Riazuelo, Phys. Rev. D **70**, 103530 (2004) [arXiv:astro-ph/0409326].
- [32] M. Beltran, J. Garcia-Bellido, J. Lesgourgues and M. Viel, Phys. Rev. D **72**, 103515 (2005) [arXiv:astro-ph/0509209].
- [33] I. Sollom, A. Challinor and M. P. Hobson, Phys. Rev. D **79**, 123521 (2009) [arXiv:0903.5257 [astro-ph.CO]].
- [34] H. Li, J. Liu, J. Q. Xia and Y. F. Cai, arXiv:1012.2511 [astro-ph.CO].
- [35] D. Baumann *et al.* [CMBPol Study Team Collaboration], AIP Conf. Proc. **1141**, 10 (2009) [arXiv:0811.3919 [astro-ph]].
- [36] M. Zaldarriaga, D. N. Spergel and U. Seljak, Astrophys. J. **488**, 1 (1997) [arXiv:astro-ph/9702157].
- [37] M. Tegmark, Phys. Rev. Lett. **79**, 3806 (1997) [arXiv:astro-ph/9706198].
- [38] Y. Mao, M. Tegmark, M. McQuinn, M. Zaldarriaga and O. Zahn, Phys. Rev. D **78**, 023529 (2008) [arXiv:0802.1710 [astro-ph]].